ONE-STEP ELECTRODEPOSITION OF SnO$_2$-Ag HYBRID FILM AND ITS PHOTOCATALYTIC PROPERTY

B. HAN, Y. LIU, X. MENG, J. NAN, W. ZHENG[*]
College of Science, Hebei North University, Zhang Jiakou, Hebei Province, 075000 China

SnO$_2$-Ag hybrid film was fabricated by a simple one-step electrodeposition method. The prepared hybrid thin film consists of SnO$_2$ nanorods with Ag nanoparticles. The synthesized hybrid thin film was characterized by SEM, XRD, UV–vis spectrophotometer, Raman spectroscopy, photoluminescence spectroscopy and photocurrent measurement. The photocatalytic activity of the SnO$_2$-Ag hybrid film was investigated by the degradation of 4-chlorophenol, methyl orange and methylene blue under visible light and compared with pure SnO$_2$ thin film. These results suggested that the Ag nanoparticles induced visible light activity and facilitated efficient charge separation in the SnO$_2$-Ag hybrid film, which displayed a superior photocatalytic performance.

1. Introduction

In the past decades, photocatalysis using semiconductor nanoparticles has been received tremendous attention for the degradation and mineralization of organic pollutants, such as ZnO, Y$_2$O$_3$, MoS$_2$, CdCoO$_3$ SnO$_2$ and TiO$_2$.[1-10] Among them, SnO$_2$ has been gained much response in the photocatalytic degradation on account of its excellent transparency, high photosensitivity, suitable band gap, low cost and environmental friendliness [11-16]. Nevertheless, like other semiconductors, the photocatalytic rate of SnO$_2$ is still limited by its electron–hole recombination. Moreover, the wide band gap of SnO$_2$ hampers its photocatalytic activity under visible light. In order to improve photocatalytic activity of SnO$_2$, efforts have been taken to manipulate other materials with SnO$_2$ such as doping with metals, non-metals and coupling with other metal oxides [17-22]. Among them, combining SnO$_2$ with noble metals has received much attention. It because the light harvesting properties of the noble metals could enhance the photocatalytic reaction under visible light irradiation. Moreover, due to the plasmon resonance phenomenon, the electrons can be excited from noble metals and transferred to the conduction band of the SnO$_2$. The electrons can assist in the formation of super-oxide radical anions and hydroxyl radicals, whereas the holes can act as redox centers to initiate the photocatalytic reactions and subsequently improve the photocatalytic performance of SnO$_2$ [23-27]. For example, Wu and co-workers used g a seed-mediated hydrothermal method for the synthesis of Au–SnO$_2$ hybrid nanostructures [28]. The photocatalytic tests showed that the Au–SnO$_2$ hybrid nanostructures exhibited enhanced visible light or UV photocatalytic abilities. Similar result also was reported by You and co-workers [29]. They deposited Au nanoparticles on the SnO$_2$ supersymmetric nanostructures and found the enhanced photocatalytic activity towards photodegradation of R6G molecules. Besides Au nanoparticles, several reports also investigated the photocatalytic performance of loading Ag nanoparticles on the SnO$_2$ due to the relatively cheap price of Ag. For example, Ansari and co-workers recently synthesized an Ag–SnO$_2$ nanocomposites in water at room temperature using an electrochemically active biofilm [26]. The results nanocomposite showed an enhanced

---

[*] Corresponding author: weizhenghnu@gmail.com

performance in the photodegradation of various organic pollutants. Wang and co-workers reported a self-assemble flower-like SnO_2/Ag heterostructures [30, 31]. The synthesized heterostructures also exhibited photocatalytic property. However the noble metal/SnO_2 photocatalysts are normally produced and used as powder which have many drawbacks in practical applications such as aggregation at high concentrations, low recycle rate and the difficulty to be segregated from reaction systems. SnO_2 based thin films are normally stable and permit transmittance. Several methods have been demonstrated for synthesizing SnO_2 based thin film, including RF sputtering technique, spray pyrolysis, sol–gel and electrodeposition [32-41]. Among these methods, the electrodeposition method exhibits many advantages, such as low operation temperature, rigid control on film thickness and morphology, relatively high deposition rate and low fabrication cost. However, to the best of our knowledge, there are no papers describing the electrodeposited noble metal/SnO_2 thin film for photocatalytic applications.

In this study, we describe a one-step electrodeposition of SnO_2-Ag hybrid thin films with superior photocatalytic properties. Tin(II) chloride dihydrate and silver nitrate were used as precursors. The prepared hybrid thin film was characterized by a series of techniques. The SnO_2-Ag hybrid thin film exhibited enhanced photocatalytic activity under visible light irradiation for degradation of methylene blue (MB), methylene orange (MO) and 4-chlorophenol (4-CP) compared with pure SnO_2 thin film. The results also indicated that the hybrid catalyst could be reused for several cycles.

2. Experimental

2.1 Materials

Tin(II) chloride dehydrate ($SnCl_2 \cdot 2H_2O$), silver nitrate ($AgNO_3$), MB, MO and 4-CP were obtained from Sigma-Aldrich. ITO slides (9 × 30 mm) were used as substrates All other chemicals used were analytical grade reagents without further purification. Milli-Q water was used throughout the experiments.

2.2 Preparation of SnO_2-Ag hybrid thin film

For electrodeposition of SnO_2-Ag hybrid thin film. A platinum wire was used as the auxiliary electrode and an Ag/AgCl (3M KCl) as the reference electrode. The electrodeposition of SnO_2-Ag film was performed using a ITO in 0.5 M HNO_3 solution containing 0.1 M $SnCl_2$ and using chronoamperometry at an applied potential of −0.7 V for 600s. The pure SnO_2 thin film was fabricated using a similar method except adding $AgNO_3$ in to electrolyte.

2.3 Characterizations

The morphology of the samples was characterised by field emission scanning electron microscope (FESEM, FEI, Quanta 400 FEG). X-ray diffraction patterns were collected from 20° to 80° in 2θ by a XRD with Cu Kα radiation (D8-Advanced, Bruker). Raman spectroscopy was performed at room temperature using a Raman Microprobe (Renishaw RM1000) with 514 nm laser light. The optical absorption was investigated using a UV–vis spectrophotometer (U-41000, HITACHI) in the range of 200–800 nm. The Photoluminescence (PL) emission curves were obtained by a Fluorescence spectrophotometer. The excitation of all analysis was set at 330 nm at room temperature and the emission curves were recorded from 340 to 950 nm. The photocurrent densities were performed on a CHI 660A electrochemical workstation. The SiO_2/ITO or SiO_2-Ag/ITO films were worked as the photoanode, Pt wire as the counter electrode, and Ag/AgCl$_3$ as the reference electrode. 0.5 M H_2SO_4 was used as electrolyte.

2.4 Photocatalytic activity evaluation

Photocatalytic properties of thin films were evaluated by using MB, MO and 4-CP as the model contaminant. A thin film coated ITO slide was placed in a plastic Petri dish containing 20 mL MO (10 mg/L) or MB (10 mg/L) or 4-CP (40 mg/L) solution with constant magnetic stirring. A 125 W high-pressure mercury lamp (with a maximum emission at about 365 nm) was used as the irradiation source. 2 mL of dye solution was taken at different illumination times and filtered through membranes of 0.45 μm pore size, the absorbance at 664 nm, 464 nm and 225 nm was recorded by UV-vis spectroscopy for determining the concentration change of MB, MO and 4-CP, respectively.

3. Results and discussion

The morphology of prepared SnO_2 and SnO_2-Ag films was characterized by SEM. As shown in Figure 1A, the SnO_2 nanostructures are mainly exhibit a rod structure with average length of 1.2 μm. In terms of SnO_2-Ag hybrid film (Figure 1B), the SnO_2 still remains a nanorod shape, however, many small Ag nanoparticles could clearly observed. The average size of Ag nanoparticles has been calculated to be 63 nm. The incorporation of Ag nanoparticles could provide a higher surface area of the thin film as well as build a connection between the SnO_2 nanorods, which is beneficial for photocatalytic application.

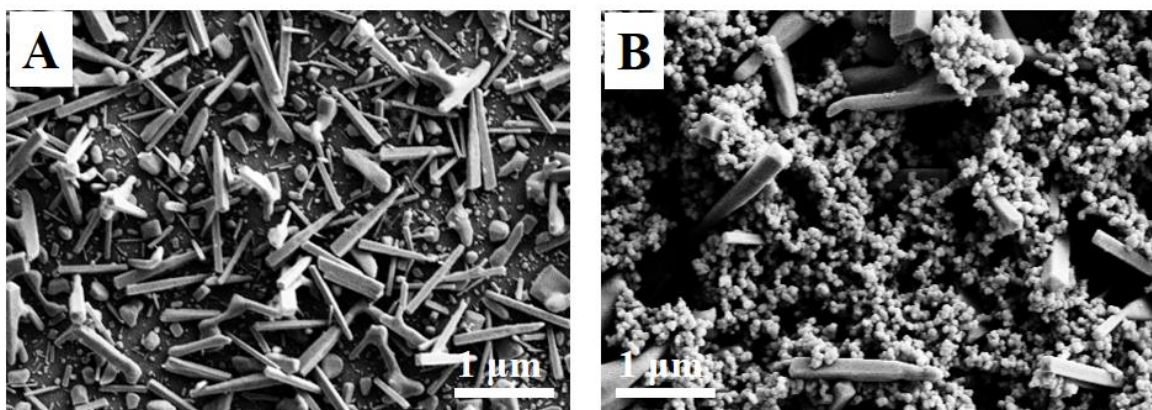*Fig. 1. SEM images of (A) pure SiO_2 and (B) SiO_2-Ag hybrid films.*

In order to obtain the elemental information about the SnO_2-Ag hybrid, EDX characterization was the carried out. Figure 2A shows the EDX spectrum of the SnO_2-Ag hybrid. The spectrum presents the only existence of Sn, O and Ag. No other impurity element was observed in the sample, indicating the high purity of the electrodeposited SnO_2-Ag hybrid. The crystalline phase composition of as-obtained hybrid was analysed by XRD. Figure 2B shows the XRD patterns of SnO_2 and SnO_2-Ag hybrid. It can be observed that the SnO_2 displays a series of characteristic peaks at 2θ of 26.53°, 33.87°, 37.93°, 38.96°, 51.69°, 54.61°, 57.71°, 61.79°, 64.30°, 65.86°, 71.05° and 78.46°, which related to the (110), (200), (111), (211), (220), (002), (310), (112), (301), (202) and (321) crystal planes of tetragonal SnO_2 (JCPDS card No. 41-1445), respectively [42]. On the other hand, the SnO_2-Ag hybrid also exhibits peaks at 2θ of 44.28°, 64.40° and 74.36°, which can be assigned to the (200), (220), (311) crystallographic plane of face centered cubic (fcc) Ag (JCPDS no. 04-0783) [28, 43, 44]. The results suggest that the one-step electrodeposition of SnO_2-Ag hybrid was successfully achieved and the incorporation of Ag nanoparticles does not change the crystalline structure of SnO_2

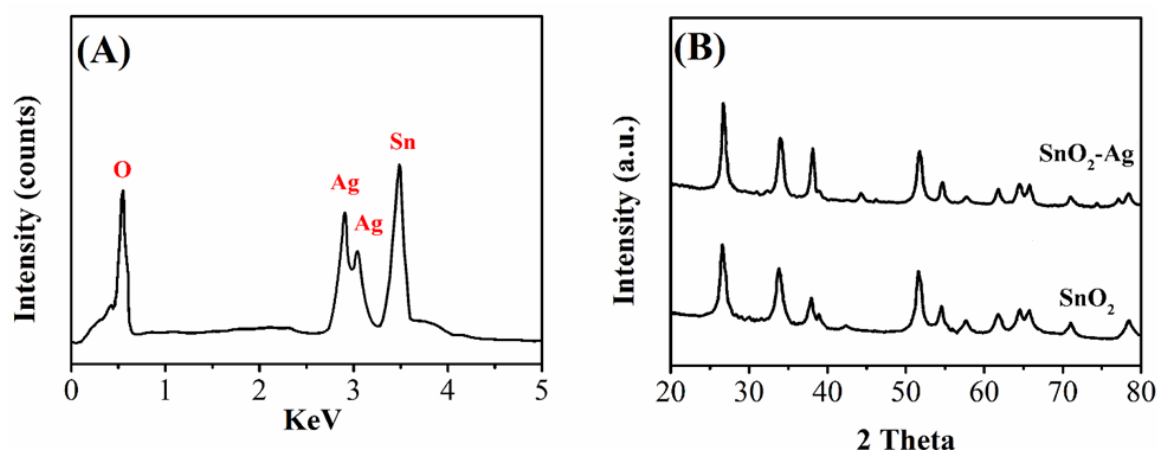*Fig. 2. (A) EDX spectrum of SiO₂-Ag hybrid film. (B) XRD patterns of pure SiO₂ film and SiO₂-Ag hybrid film.*

Fig. 3A shows the UV-vis spectra of the SnO_2 and SnO_2-Ag hybrid. It can be seen that the absorbance of the SnO_2 nanorods are mainly in the UV range due to their wide band gap. While the SnO_2-Ag hybrid exhibits a significant peak from 380–450 nm, which can be indexed to the surface plasmon resonance absorption of Ag nanoparticles [45-47]. further confirming the successful formation of SnO_2-Ag hybrid.

Figure 3B shows the Room-temperature Raman spectra of SnO_2 and SnO_2-Ag hybrid. As expect, a large peak is observed at 625 cm^{-1}, which is attributed to the A_{1g} vibration mode of SnO_2 with tetragonal rutile structure [48]. After incorporation with Ag nanoparticles, the spectrum of the SnO_2-Ag hybrid exhibits several peaks at around 450 and 650 cm^{-1}, which could due to the increased defects of nanocrystallites such as oxygen vacancies, vacancy clusters, strains and local lattice disorder at the interface and interior surface related to the effect of additional Ag [30, 49, 50]. Also, it could ascribe to the electron transfer between SnO_2 and Ag nanoparticles.
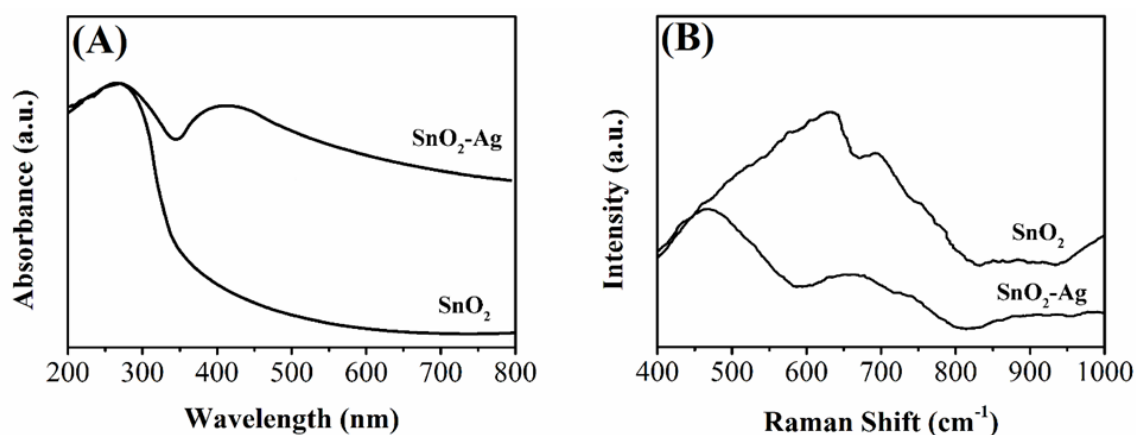

Fig. 3. (A) UV-visible diffuse reflectance spectra and (B) Raman spectra of SiO₂ and SiO₂-Ag hybrid films.

Fig. 4A shows the room temperature PL spectra of SnO_2 and SnO_2-Ag hybrid. Both spectra present a wide emission band in the wavenumber range from 340 to 950 nm. However, the spectrum of the SnO_2 exhibits a much stronger emission intensity compared with that of the SnO_2-Ag hybrid, confirming the fastest charge recombination rate [51]. The synergistic effect between the semiconductor and noble metals could effectively reduce the electro hole pairs recombination thus facilitate the charge carrier separation. It can be seen that the PL intensity is reduced significantly after the incorporation with Ag nanoparticles due to the efficient charge separation

and the inhibited electron-hole recombination. Because the SnO_2-Ag hybrid represents the lower PL emission band, which may lead to a higher photocatalytic activity.

The photocurrent responses of SnO_2 and SnO_2-Ag hybrid film were measured under visible light illumination using ITO as substrate and the results are presented in Figure 4B. The results suggest that the SnO_2 and SnO_2-Ag hybrid film both exhibit clearly current responses upon visible light illumination. It is worth noting that the SnO_2-Ag hybrid film exhibits a much larger photocurrent compared than that of the pure SnO_2 film, further suggesting that the incorporation of Ag with SnO_2 could effectively suppress photogenerated electron hole pair recombination.
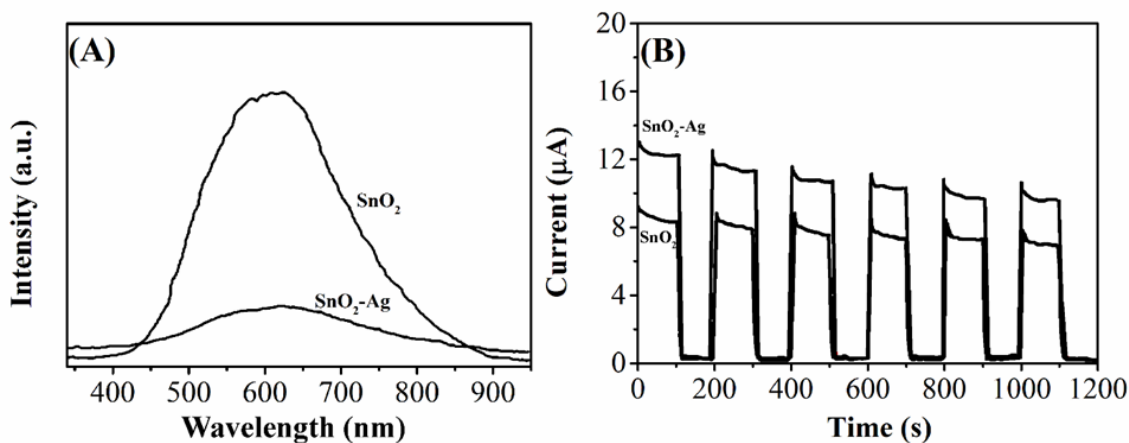

Fig. 4. (A) Room-temperature PL spectra of SiO_2 and SiO_2-Ag hybrid thin film with an excitation wavelength of 330 nm. (B) Photocurrent densities vs. time for the SiO_2 and SiO_2-Ag hybrid film under visible light illumination.

The photocatalytic activities of the as-prepared photocatalysts were evaluated by photodegradation of MB, MO and 4-CP. Figure 5 shows the degradation (C/C_0) of MB, MO and 4-CP as a function of the irradiation time, where C_0 and C are the initial concentration of the organic compound and concentration after visible light irradiation. As shown in the figure, the MB, MO and 4-CP were hardly decomposed by visible light irradiation in the absence of photocatalyst. In contrast, after visible light irradiation on MB, MO and 4-CP for 4 h, 5 h and 5 h in the presence of pure SnO_2 thin film, respectively, 58% of MB, 46% of MO and 39% of CP were degraded. On the other hand, almost complete degradation of MB, MO and 4-CP occurred when the presence of SnO_2-Ag hybrid thin film under the same conditions. The first-order kinetic linear simulation curves of different photocatalysts for three organic pollutant degradation are presented in Figure 6. The rate constants of the pure SnO_2 film and SnO_2-Ag hybrid film for the degradation of MB are 0.003615/min and 0.009831/min, respectively. The rate constants of the pure SnO_2 film and SnO_2-Ag hybrid film for the degradation of MO are 0.002029/min and 0.006134/min, respectively. Similarly, the rate constants of the pure SnO_2 film and SnO_2-Ag hybrid film for the degradation of 4-CP are 0.001642/min and 0.005221/min, respectively. Therefore, the SnO_2-Ag hybrid film exhibits enhanced visible light photocatalytic activity compared to pure SnO_2 film. The reason of the enhanced photocatalytic activity could ascribe to the synergistic effect between the SnO_2 and the surface plasmon resonance effect of the Ag nanoparticles. Under visible light irradiation, the electron hole pairs will generate on the surface of the Ag nanoparticles due to the excitation of the surface plasmon resonance of the Ag nanoparticles. The electrons transfer rapidly occurs from Ag to SnO_2 through the interface between two materials [52]. These electrons will be trapped by dissolved oxygen molecules to yield oxidative species, such as super-oxide radical anions ($^\bullet O2^-$) and hydroxyl radicals ($HO^\bullet$). On the other hand, the holes on the surface of the Ag nanoparticles will be trapped by OH^- to result $HO^\bullet$ species. Moreover, the trapping nature of the Ag nanoparticles also yields in the production of more super oxide radical anions. The detail degradation process of organic pollutant can be expressed as follow: under light illumination, the photogenerated electrons in organic molecules will be captured by the adsorbed O_2 and form O_2^-.

248

H_2O_2 is formed by the reaction between O_2^- and electron. Then, the H_2O_2 can further react with the electrons to produce OH^- and $HO^•$. The $HO^•$ can also be formed through the reaction of holes with OH^-. The organic molecules absorbed on the photocatalyst can be oxidized by several ways, including react with O^-, $HO^•$ and holes. Eventually, the organic molecules can be photodegraded into CO_2 and H_2O.

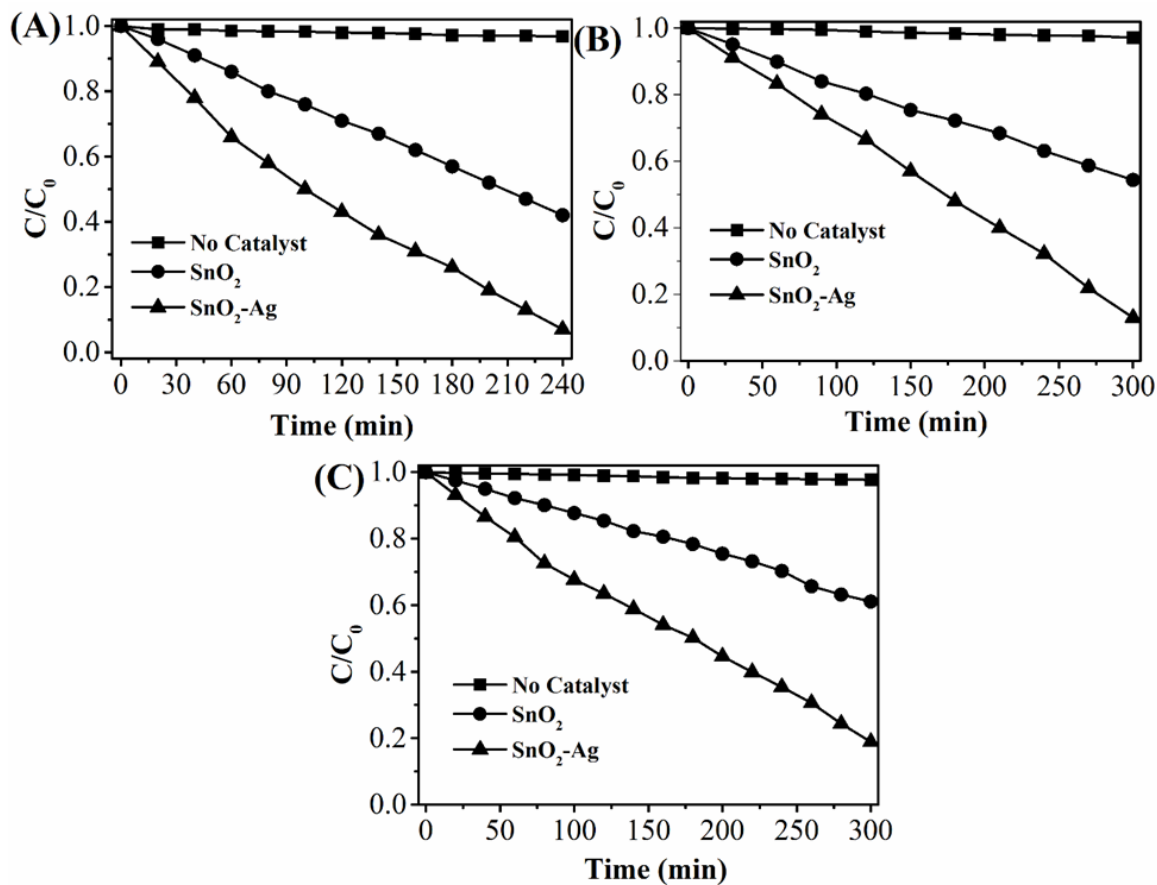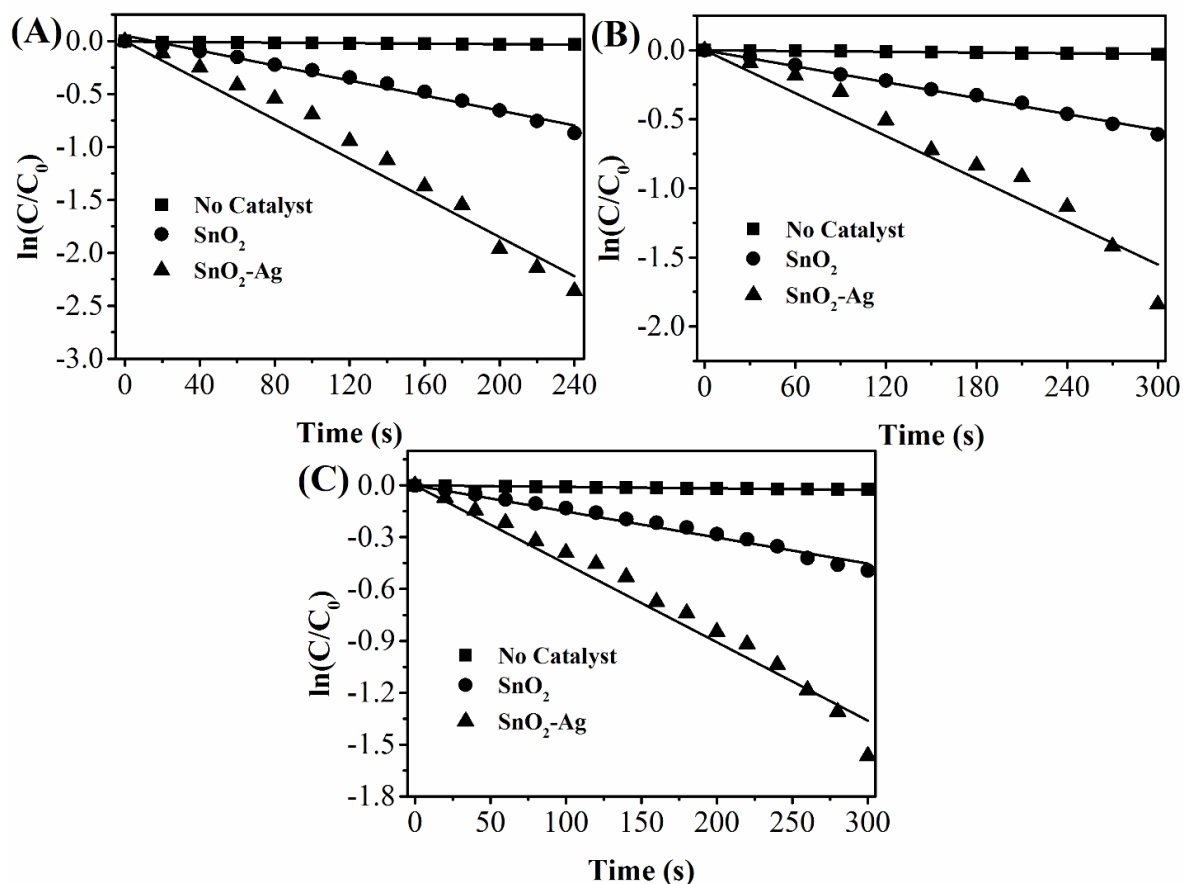*Fig. 5. Comparison of (A) MB, (B) MO and (C) 4-CP photodegradation in the presence of different photocatalysts.*

Fig. 6. ln(C/C₀) vs. time (h) plot for the photodegradation of (A) MB, (B) MO and (C) 4-CP by absence of photocatalyst, pure SiO₂ film and SiO₂-Ag hybrid film.

4. Conclusion

In this study, SnO₂-Ag hybrid film was successfully fabricated by a simple electrodeposition method using SnCl₂ and AgNO₃ as precursor. A series of characterizations indicated the proposed method could produce a high quality SnO₂-Ag hybrid film. The as-prepared hybrid film exhibited a much higher photocatalytic activity for MB, MO and 4-CP degradation under visible light irradiation than that of SnO₂ film due to the synergistic effect between two materials. In conclusion, the electrodeposited SnO₂-Ag hybrid film is a suitable candidate for photodegradation organic pollutant, which could apply for fabricating self-cleaning surface.

Reference

[1] T.R. Giraldi, G.V.F. Santos, V.R. De Mendonca, C. Ribeiro, I.T. Weber, Mater. Chem. Phys. **136,** 505 (2012).
[2] C. Karunakaran, R. Dhanalakshmi, P. Anilkumar, J. Hazard. Mater. **167,** 664 (2009).
[3] J.P. Wilcoxon, Journal of Physical Chemistry B **104,** 7334 (2000).

[4] P.K. Baitha, P.P. Pal, J. Manam, Nuclear Instruments and Methods in Physics Research Section A: Accelerators, Spectrometers, Detectors and Associated Equipment **745,** 91 (2014).

[5] L. Fu, Z. Fu, Ceram Int **41,** 2492 (2015).

[6] K. Vignesh, R. Hariharan, M. Rajarajan, A. Suganthi, Solid State Sciences **21,** 91 (2013).

[7] L. Fu, Y. Zheng, Q. Ren, A. Wang, B. Deng, Journal of Ovonic Research **11,** 21 (2015).

[8] C. Sima, L. Ion, C. Grigoriu, T.L. Mitran, S. Antonhe, Digest Journal of Nanomaterials and Biostructures **9,** 1479 (2014).

[9] N. Preda, M. Enculescu, A. Florica, A. costas, A. eEvanghelidis, E. Matei, I. Enculescu, Digest Journal of Nanomaterials and Biostructures **8,** 1590 (2014).

[10] G.H. Tariq, N.A. Niaz, M. Anis-Ur-Rehman, Chalcogenide Letters **11,** 461 (2014).

[11] R. Yang, Y. Gu, Y. Li, J. Zheng, X. Li, Acta Materialia **58,** 866 (2010).

[12] W. Zhou, R. Liu, Q. Wan, Q. Zhang, A.L. Pan, L. Guo, B. Zou, J Phys Chem C **113,** 1719 (2009).

[13] Y. Hao, W. Wenjie, X. Lili, Preparation and photocatalytic properties of nanometer SnO_2, Chemical, Biological and Environmental Engineering (ICBEE), 2010 2nd International Conference on, 2010, pp. 96.

[14] X. Sun, R. Long, X. Cheng, X. Zhao, Y. Dai, B. Huang, J Phys Chem C **112,** 9861 (2008).

[15] Z.L. Zhang, M.L. Wang, Y.L. Mao, Mater. Technol. **30,** 2 (2014).

[16] K. Wang, Y. Huang, H.J. Huang, M. Zong, J. Ding, Y.L. Wang, Mater. Technol. **30,** 7 (2014).

[17] Y. Wang, C.-m. Fan, B. Hua, Z.-h. Liang, Y.-p. Sun, Transactions of Nonferrous Metals Society of China **19,** 778 (2009).

[18] H.-l. Xia, H.-s. Zhuang, T. Zhang, D.-c. Xiao, Journal of Environmental Sciences **19,** 1141 (2007).

[19] S. Pan, S. Wang, Y. Zhang, S. Xu, F. Kong, Y. Luo, Y. Tian, X. Teng, G. Li, Catalysis Communications **24,** 96 (2012).

[20] L.-P. Zhu, N.-C. Bing, D.-D. Yang, Y. Yang, G.-H. Liao, L.-J. Wang, CrystEngComm **13,** 4486 (2011).

[21] H. Xia, H. Zhuang, T. Zhang, D. Xiao, Materials Letters **62,** 1126 (2008).

[22] N. Soltani, A. Dehzangi, A. Kharazmi, E. Saion, W.M.M. Yunus, B.Y. Majlis, M.R. Zare, E. Gharibshahi, N. Khalilzadeh, Chalcogenide Letters **11,** 79 (2014).

[23] P. Wang, B. Huang, Y. Dai, M.-H. Whangbo, Phys Chem Chem Phys **14,** 9813 (2012).

[24] L. Jing, W. Zhou, G. Tian, H. Fu, Chemical Society Reviews **42,** 9509 (2013).

[25] S.T. Kochuveedu, Y.H. Jang, D.H. Kim, Chemical Society Reviews **42,** 8467 (2013).

[26] S.A. Ansari, M.M. Khan, M.O. Ansari, J. Lee, M.H. Cho, RSC Advances **4,** 26013 (2014).

[27] Z. Khan, T.R. Chetia, A.K. Vardhaman, D. Barpuzary, C.V. Sastri, M. Qureshi, RSC Advances **2,** 12122 (2012).

[28] W. Wu, L. Liao, S. Zhang, J. Zhou, X. Xiao, F. Ren, L. Sun, Z. Dai, C. Jiang, Nanoscale **5,** 5628 (2013).

[29] H. You, R. Liu, C. Liang, S. Yang, F. Wang, X. Lu, B. Ding, Journal of Materials Chemistry A **1,** 4097 (2013).

[30] X. Wang, H. Fan, P. Ren, Colloids and Surfaces A: Physicochemical and Engineering Aspects **419,** 140 (2013).

[31] M.M. Byranvand, A.N. Kharat, Journal of Ovonic Research **10,** 191 (2014).

[32] L. Fu, A. Yu, Carbon nanotube based nanostructured thin films: preparation and application, Fourth International Conference on Smart Materials and Nanotechnology in Engineering, International Society for Optics and Photonics, 2013, pp. 87930T.

[33] L. Fu, J. Yong, G. Lai, T. Tamanna, S. Notley, A. Yu, Materials and Manufacturing Processes **29,** 1030 (2014).

[34] P. Tyagi, A. Sharma, M. Tomar, V. Gupta, Advanced Science Letters **20,** 953 (2014).

[35] B. Zhang, Y. Tian, J.X. Zhang, W. Cai, Journal of Materials Science **46,** 1884 (2011).

[36] K. Joy, S.S. Lakshmy, P.V. Thomas, Journal of Sol-Gel Science and Technology **61,** 179 (2012).

[37] L. Fu, A. Wang, Y. Zheng, W. Cai, Z. Fu, Materials Letters **142,** 119 (2015).

[38] A. Wang, H.P. Ng, Y. Xu, Y. Li, Y. Zheng, J. Yu, F. Han, F. Peng, L. Fu, Journal of Nanomaterials **2014,** 6 (2014).

[39] G. Liu, Z. Zhao, X. Jiao, D. Chen, Mater. Technol. **29,** 167 (2013).

[40] L. Fu, T. Tamanna, W.-J. Hu, A. Yu, Chemical Papers **68,** 1283 (2014).

[41] I. M.A., K.S. Rahman, F. Haque, N. Dhar, M. Salim, M. Akhtaruzzaman, K. Sopian, N. Amin, Journal of Ovonic Research **10,** 185 (2014).

[42] S.A. Ansari, M.M. Khan, M. Omaish Ansari, J. Lee, M.H. Cho, New J Chem **38,** 2462 (2014).

[43] M.M. Khan, S.A. Ansari, M.O. Ansari, B.K. Min, J. Lee, M.H. Cho, J Phys Chem C **118,** 9477 (2014).

[44] S.A. Ansari, M.M. Khan, J. Lee, M.H. Cho, Journal of Industrial and Engineering Chemistry **20,** 1602 (2014).

[45] S. Hajizadeh, K. Farhadi, M. Forough, R.E. Sabzi, Analytical Methods **3,** 2599 (2011).

[46] Y. Zhang, S. Liu, L. Wang, X. Qin, J. Tian, W. Lu, G. Chang, X. Sun, RSC Advances **2,** 538 (2012).

[47] T. Wu, S. Liu, Y. Luo, W. Lu, L. Wang, X. Sun, Nanoscale **3,** 2142 (2011).

[48] G. Cheng, K. Wu, P. Zhao, Y. Cheng, X. He, K. Huang, Journal of Crystal Growth **309,** 53 (2007).

[49] Q.-Y. Wen, H.-W. Zhang, Q.-H. Yang, Y.-Q. Song, J.Q. Xiao, Journal of Magnetism and Magnetic Materials **321,** 3110 (2009).

[50] K.N. Yu, Y.H. Xiong, Y.L. Liu, C.S. Xiong, Physical Review B **55,** 2666 (1997).

[51] J. Liqiang, Q. Yichun, W. Baiqi, L. Shudan, J. Baojiang, Y. Libin, F. Wei, F. Honggang, S. Jiazhong, Solar Energy Materials and Solar Cells **90,** 1773 (2006).

[52] Z. Chen, L. Fang, W. Dong, F. Zheng, M. Shen, J. Wang, Journal of Materials Chemistry A **2,** 824 (2014).